Age-Related Macular Degeneration Detection and Stage Classification using Choroidal OCT Images

Jingjing Deng[1], Xianghua Xie[1]*, Louise Terry[2], Ashley Wood[2], Nick White[2], Tom H. Margrain[2], and Rachel V. North[2]

1. Department of Computer Science, Swansea University
Singleton Park, Swansea SA2 8PP, United Kingdom
*x.xie@swansea.ac.uk
http://csvision.swan.ac.uk

2. School of Optometry and Vision Sciences, Cardiff University
Cathays, Cardiff CF24 4HQ, United Kingdom

Abstract. Age-Related Macular Degeneration (AMD) is a progressive eye disease which damages the retina and causes visual impairment. Detecting those in the early stages at most risk of progression will allow more timely treatment and preserve sight. In this paper, we propose a machine learning based method to detect AMD and distinguish the different stages using choroidal images obtained from optical coherence tomography (OCT). We extract texture features using a Gabor filter bank and non-linear energy transformation. Then the histogram based feature descriptors are used to train the random forests, Support Vector Machine (SVM) and neural networks, which are tested on our choroid OCT image dataset with 21 participants. The experimental results show the feasibility of our method.

Keywords: AMD diseases classification, choroidal OCT image, texture analysis.

1 Introduction

Age-Related Macular Degeneration is the leading cause of sight loss and visual impairment among older adults (above 55 years) [5]. It affects the outer retinal layers, particularly the photoreceptors, retinal pigment epithelium (RPE) and choroid, leading to central vision loss. The exact cause of AMD is still not fully understood, but is known to be multifactorial, with increasing age being the most consistent factor [1]. The condition can be clinically categorised into three stages. An early stage, where vision is relatively unaffected, that may progress to one of two advanced stages: dry (atrophic) AMD or wet (neovascular) AMD. In both end stages, the choroid is affected. The wet AMD subtype is characterised by growth of new blood vessels from the choroid into the retina, forming a choroidal neovascular membrane (CNVM). These vessels are prone to leakage

causing oedema, haemorrhage, and in some cases pigment epithelial detachments (PED). These changes result in sudden and severe loss of central vision. The dry AMD subtype represents an atrophy of the RPE retina, and loss of choroidal vasculature. Currently, optical coherence tomography (OCT) imaging of the retina is the gold standard diagnostic technique for this condition. However, advances in OCT now allow us to visualise the deeper structures, including the choroid. Histology has shown these choroidal vessels to have changed substantially in advanced AMD [19]. Detecting these changes in *vivo* particularly in early disease may improve detection of AMD, prior to retinal damage.

To detect textural changes to the vasculature in these images, machine learning and pattern recognition techniques, such as random forests, SVM and neural networks, can be applied. These machine learning algorithms have been shown effective in various classification problem, for example, distinguishing different human conversational scenarios [7], segmenting the region of interest in OCT and IVUS images [13, 9]. Random forests [4] is an ensemble learning method, it grows a number of decision trees independently using the subsets which are randomly sampled from the complete training set with replacement. During the classification stage, the testing sample walks through each decision tree by evaluating its features at non-leaf node, and finally reaches a leaf node at the bottom, which votes the class with largest proposition of training samples it holds. The random forests combine all voting results from individual decision trees, and assigns the most voted class to the testing sample. SVM [6] separates the samples by mapping the feature into high dimensional space and finding the separation hyper-planes for different classes. The testing sample is represented in the high dimensional space using the same mapping function, and its class is determined by the region it falls on, which is bounded by the hyper-planes. Neural networks [11] consider the supervised classification as a function fitting problem given the input feature as argument, and the prediction as function value. Then the unknown function can be learned by approximating with one or more layers of interconnected neurons organised hierarchically. Recently, deep neural networks have shown great learning capacity and higher accuracy compared with the traditional learning methods in almost all aspects of pattern recognition [17].

Koprowski et al. [14] proposed a method to classify choroidal OCT images into pre-defined clinical conditions by extracting high level features, such as number of detected objects, and average position of the centre of gravity, from low level texture information. Whereas, in this paper we present a method using the low level texture features not only to detect disease, but also to categorise into broadly defined AMD disease stages instead of specific clinical conditions. The rest of this paper is organised as follows. Sec. 2 provides the the details of the OCT image acquisition procedure, Sec. 3 presents our proposed method including feature extraction, and classifier training. The experimental results are illustrated and discussed in Sec. 4. Sec. 5 concludes the work, and presents the future plan.

2 Data

Participants were recruited with dry AMD (n=7, Age=80.00±9.95) and wet AMD (n=7, Age=82.00±4.43), along with a group of healthy age-similar controls (n=7, Age=68.85±6.64). In order to avoid any bias which may be introduced by having a predominant class, we imaged 7 participants for each class. All participants underwent long-wavelength OCT imaging using a 1060nm light source. This wavelength penetrates deeper into the retina and choroid, allowing visualization of the deeper structures, and also benefits from reduced intra-ocular scattering caused by media opacities such as cataract [18]. Firstly, the length of the participants eyes were measured, and then followed by 20°x20° (512 x 512 x 1024) volume scan, This is approximately 10.3mm wide given a mean axial eye length of 24.46mm. The images were scaled laterally using the measured axial eye length of each patient, the scan angle and assumed refractive index of the ocular media.

All OCT images were collected by a single trained operator (AW), and classified by three experienced, masked observers into three groups: normal, dry AMD, and wet AMD. The classifications were based on the retinal appearance and Age-Related Eye Disease Study definitions of disease progression [2]. This was taken as ground truth. For each image, 100 slices of the choroid regions were labelled, 20 of which were randomly selected and used in training and testing. For the control group, 20 slices out of 512 for each participant were randomly chosen. Thus, we had a total of 420 images in total with the choroidal region labelled as a closed contour. Fig. 1 shows examples of OCT images from each groups.

3 Method

In this paper, we proposed a machine learning-based method to detect AMD and distinguish the different stages using choroidal OCT imaging. To our knowledge, this is the first work testing the feasibility of classifying AMD by choroidal appearance in OCT images. At the dry stage of AMD the first sign includes the accumulating of drusen between retina and Bruch's membrane. The choroid is affected in the progression to both Wet & Dry subtypes, either as the source of new blood vessels that invade the retina (Wet) or through a progressive loss of vasculature (Dry). These pathological processes affect the textural appearance of choroid sections on the OCT image. The problem of detecting the AMD and distinguishing different stages can be approached as a texture classification problem. However, the changes of texture appearance are subtle, and often not noticeable. To tackle this problem, Gabor filtering followed by an energy transformation was employed to detect frequency information of the input images within different scales and orientations. The histogram of energy responses were used to form the feature descriptors for pre-labelled choroid regions. Given the ground truth of AMD stage, a set of classifiers were trained in a supervised fashion, which will be used for AMD classification. The flowchart shown in Fig. 2 illustrates the steps from preprocessing, to feature extraction, to classification.

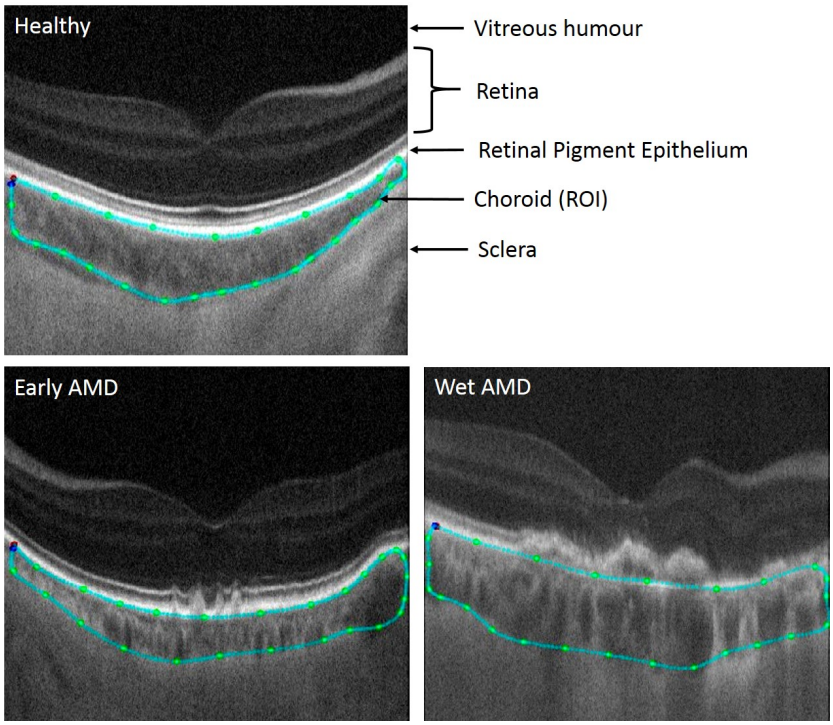

Fig. 1. Three example OCT images representing the 3 classification groups used as ground truth. The green contours were labelled manually highlighting the choroid regions of interest (ROI).

3.1 Feature extraction and descriptors

Gabor filters have been widely used in texture analysis [20, 10], especially in surface defects detection [22, 15, 16, 3] and image segmentation [8, 21], due to its capacity of representing the frequency and orientation information which is fairly similar to the human visual perception. In our case, we used 2D Gabor filter which could be defined by a complex sinusoid multiplied by a Gaussian function. For images, the Gabor responses can be computed by convolving the image matrix with the Gabor filter matrix which is simply obtained by sampling at discrete coordinates from the continuous Gabor function. To compute the feature image in multi-scales, we filtered the image using a Gabor filter bank first, and then applied an energy transformation proposed by Jain et al. [12] to the responses, where the responses are subjected to a bounded non-linearity (Eqn. 1), and then followed by convolving with a square averaging kernel (Eqn. 2).

$$\psi(g) = tanh(\alpha g) = \frac{1 - e^{-2\alpha g}}{1 + e^{-2\alpha g}} \tag{1}$$

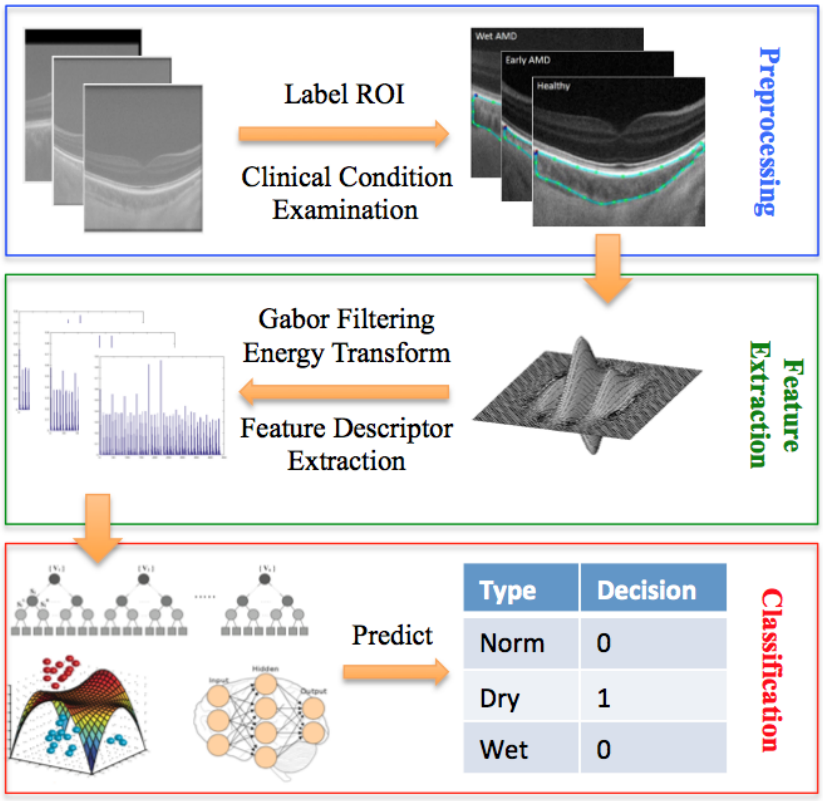

Fig. 2. Flowchart of the proposed method.

$$\mathcal{E}(C_x, C_y) = \frac{1}{S^2} \sum_{(a,b) \in W_{C_x C_y}} | \psi(g(a,b)) | \tag{2}$$

where g is Gabor function, $W_{C_x C_y}$ is the averaging window with size of $S \times S$ pixels, and centred at (C_x, C_y) image coordinate.

The labelled choroid layers varied greatly in shape thickness and appearance between individuals, as illustrated in Fig. 1. In (dry) AMD we initially expected the choroid, and consequently its texture, to be affected locally. Examining the small patches from the labelled region is not a reasonable way to diagnose the disease, as considerable amount of patches will have quite similar feature pattern, which to some extent introduces a large amount of noise to the training stage. Instead of considering local features, the histogram of the texture energy of the labelled choroid region are computed as the feature descriptors. As the feature image is bounded within [0, 1] (Eqn. 1, 2), the histogram can be computed without any further normalisation. The feature descriptors were formed by concatenating histograms of the energy image of different scales and orientations consistently.

3.2 Supervised Classification

Random forests and SVM are traditional data-driven discriminative models for supervised classification problems. The feature descriptors were designed for representing the distributions of edges at different scales and orientations. Random forests treat each feature as an independent component, whereas SVM finds the manifold in higher dimensional space by correlating the features, where the data from different classes is separable. These two classifiers are used to test the discriminative power of the feature descriptors extracted based on lower level image texture information. Neural networks can learn the high level representations of features from the inputs hierarchically, and then generalize more abstract descriptors in an unsupervised fashion. The supervised classification is carried out by stacking the SoftMax layer on the top, and back-propagating the prediction error back to the lower layers to optimize the weights of neurons. It was used to investigate the possibility of generalizing higher representation based on the hand crafted feature descriptors, where it is important in the case of modelling across individuals. Random forests, SVM and neural networks were trained separately using the same training set and feature descriptors during the learning procedure. The classification results on the testing set of individual classifiers are reported and discussed in Sec. 4.

4 Experiment and Discussion

Fig. 3 shows an example OCT image, and the corresponding energy feature images obtained by first convolving the image with Gabor filter bank and then applying the non-linear energy transformation, as described in Sec. 3.1. The Gabor filter bank is created from the initial 39 by 39 pixels 2D Gabor filter with 5 levels of scale and 8 orientations (every 45 degrees). The top row of Fig. 2(b) shows the energy responses from different orientations of the first scale, and the bottom row is obtained from the last scale. It clearly shows that the Gabor filter bank detects the edge of different orientation from fine level to coarse level. We extracted the histogram of the energy feature images for the labelled choroid region with 11 bins, and then concatenated the histograms across scales and orientations, which forms a feature descriptor vector with 440 components. Then, a random forests with 50 decision trees, an SVM with radial basis function kernel, and a shallow neural networks with one hidden layer and 360 neurons were trained and tested using the feature descriptors independently.

To carry out the classification, 10-fold cross validation was adopted, that is, the whole dataset was evenly partitioned into ten randomly sampled subsets across different patients, and one subset was retained for testing, the remaining 9 subsets were used to train the classifier. Tables 1,2,3 show the confusion matrices of random forests, SVM and neural networks, and the average of 94.7%, 97.1%, and 84.7% were achieved respectively. A significant accuracy difference was found between neural networks and other two classifiers. The neural network is suitable for learning the hierarchical representation of the features from the raw image patches such as conventional photographs which have relatively high intensity

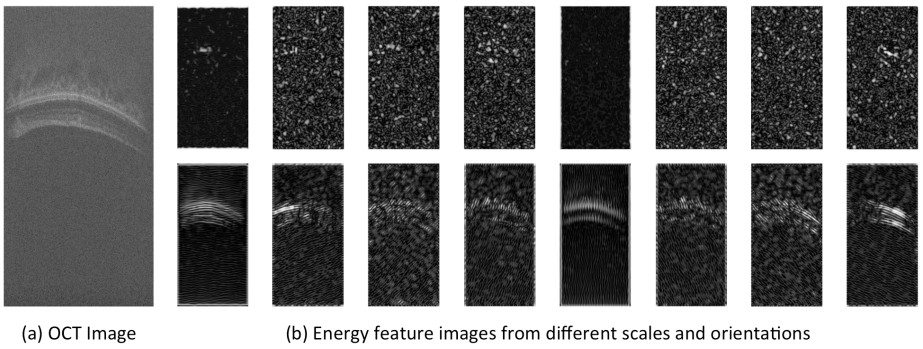

Fig. 3. (a) shows the original OCT image; (b) shows the energy feature images obtained by filtering the original image with different scales and orientations of Gabor filters. The Gabor filters are applied to the whole image first as shown in figures, and then only the choroid sections which were manually labelled beforehand are used in the study.

contrast. In our case, we employed the Gabor filter bank to detect the edge based feature, and then used histograms to generalise it. Using such feature descriptors, the discriminative models trained by finding the separation boundary should outperform the generalization model. Furthermore, 2-Fold cross validation was carried out, and the results are reported in Table 4. We observed the decrease of average accuracy of all classifiers, especially random forest, which is caused by reducing the proposition of the training set. However, the results strongly suggest that it is feasible to detect AMD pathological changing the choroid and distinguish different stages of disease by examining the image texture of the choroid.

Table 1. Confusion matrix of 10-Fold random forests (%).

	Normal	Dry AMD	Wet AMD
Normal	99.0±2.5	3.5	0.3
Dry	0.7	87.0±9.1	1.6
Wet	0.3	9.5	98.1±4.2

Table 2. Confusion matrix of 10-Fold SVM (%).

	Normal	Dry AMD	Wet AMD
Normal	96.5±4.8	0.0	1.9
Dry	0.0	97.4±4.5	0.7
Wet	3.5	2.6	97.4±3.9

Table 3. Confusion matrix of 10-Fold neural networks (%).

	Normal	Dry AMD	Wet AMD
Normal	86.5±9.3	7.3	5.1
Dry	6.6	80.8±10.2	8.1
Wet	6.9	11.9	86.8±8.3

Table 4. Classification results of 2-Fold cross validation (%).

	Normal	Dry AMD	Wet AMD	Ave.
R.F.	95.4	80.0	90.8	88.7
SVM	95.3	93.1	94.7	94.4
N.N.	80.3	73.1	81.0	78.1

5 Conclusion

In this paper, we have presented a machine learning-based method to detect and distinguish different stages of AMD using choroidal OCT imaging. The experimental results show the feasibility of the proposed method, where a computer-aided AMD classification system can be built. However, a larger dataset is necessary to account for large within-group variation, particularly in the early disease stage. This will be addressed in our future work.

References

1. Ambati, J., Fowler, B.J.: Mechanisms of age-related macular degeneration. Neuron 75(1), 26–39 (2012)
2. AREDS: The age-related eye disease study system for classifying age-related macular degeneration from stereoscopic color fundus photographs: the age-related eye disease study report number 6. American Journal of Ophthalmology 132(5), 668 – 681 (2001)
3. Bodnarova, A., Bennamoun, M., Latham, S.: Optimal gabor filters for textile flaw detection. Pattern Recognition 35(12), 2973 – 2991 (2002)
4. Breiman, L.: Random forests. Machine Learning 45(1), 5–32 (2001)
5. Bunce, C., Zekite, A., Walton, S., Rees, A., Patel, P.: Certifications for sight impairment due to age related macular degeneration in England. Public Health 129(2), 138 – 142 (2015)
6. Cortes, C., Vapnik, V.: Support-vector networks. Machine learning 20(3), 273–297 (1995)
7. Deng, J., Xie, X., Daubney, B.: A bag of words approach to subject specific 3d human pose interaction classification with random decision forests. Graphical Models 76(3), 162–171 (2014)
8. Dunn, D., Higgins, W.E.: Optimal gabor filters for texture segmentation. IEEE Transactions on Image Processing 4(7), 947–964 (1995)

9. Essa, E., Xie, X., Jones, J.L.: Minimum s-excess graph for segmenting and tracking multiple borders with HMM. In: Medical Image Computing and Computer-Assisted Intervention. pp. 28–35. Springer (2015)
10. Grigorescu, S.E., Petkov, N., Kruizinga, P.: Comparison of texture features based on gabor filters. IEEE Transactions on Image Processing 11(10), 1160–1167 (Oct 2002)
11. Hinton, G.E., Salakhutdinov, R.R.: Reducing the dimensionality of data with neural networks. Science 313(5786), 504–507 (2006)
12. Jain, A.K., Farrokhnia, F.: Unsupervised texture segmentation using gabor filters. In: IEEE International Conference on Systems, Man and Cybernetics. pp. 14–19 (1990)
13. Jones, J.L., Xie, X., Essa, E.: Combining region-based and imprecise boundary-based cues for interactive medical image segmentation. International journal for numerical methods in biomedical engineering 30(12), 1649–1666 (2014)
14. Koprowski, R., Teper, S., Wróbel, Z., Wylegala, E.: Automatic analysis of selected choroidal diseases in OCT images of the eye fundus. Biomedical engineering online 12(1), 117 (2013)
15. Kumar, A., Pang, G.K.: Defect detection in textured materials using gabor filters. IEEE Transactions on Industry Applications 38(2), 425–440 (Mar 2002)
16. Kumar, A., Pang, G.K.: Defect detection in textured materials using optimized filters. IEEE Transactions on Systems, Man, and Cybernetics, Part B: Cybernetics 32(5), 553–570 (2002)
17. LeCun, Y., Bengio, Y., Hinton, G.E.: Deep learning. Nature 521(7553), 436–444 (2015)
18. Povazay, B., Bizheva, K., Hermann, B., Unterhuber, A., Sattmann, H., Fercher, A., Drexler, W., Schubert, C., Ahnelt, P., Mei, M., et al.: Enhanced visualization of choroidal vessels using ultrahigh resolution ophthalmic OCT at 1050 nm. Optics Express 11(17), 1980–1986 (2003)
19. Spraul, C.W., Lang, G.E., Grossniklaus, H.E., Lang, G.K.: Histologic and morphometric analysis of the choroid, bruch's membrane, and retinal pigment epithelium in postmortem eyes with age-related macular degeneration and histologic examination of surgically excised choroidal neovascular membranes. Survey of ophthalmology 44, S10 – S32 (1999)
20. Xie, X.: A review of recent advances in surface defect detection using texture analysis techniques. ELCVIA Electronic Letters on Computer Vision and Image Analysis 7(3) (2008)
21. Xie, X., Mirmehdi, M.: Colour image segmentation using texems. Annals of the BMVA 1(6), 1–10 (2007)
22. Xie, X., Mirmehdi, M.: Texems: Texture exemplars for defect detection on random textured surfaces. Pattern Analysis and Machine Intelligence, IEEE Transactions on 29(8), 1454–1464 (2007)